

Surface urban heat island of Iași city (Romania) and its differences from *in situ* screen-level air temperature measurements

Lucian SFÎCĂ^a, Claudiu-Ştefănel CREȚU^{b,*}, Pavel ICHIM^c, Robert HRIȚAC^b, Iuliana-Gabriela BREABAN^a

^a Associate Professor PhD, Department of Geography, Faculty of Geography and Geology, Alexandru Ioan Cuza University of Iași, Romania

^b PhD Student, Department of Geography, Faculty of Geography and Geology, Alexandru Ioan Cuza University of Iași, Romania

^c Lecturer PhD, Department of Geography, Faculty of Geography and Geology, Alexandru Ioan Cuza University of Iași, Romania



ARTICLE INFO

Keywords:

Surface urban heat island
Canopy layer urban heat island
Land surface temperature
Atmospheric circulation types
Land use categories

ABSTRACT

Nowadays, in the field of urban climate there is a scientific need to compare Land Surface Temperature (LST) with screen-level air temperature (2mTair). This is done in our study for Iași city, based on MODIS imagery and *in situ* observations. We assess firstly the Surface Urban Heat Island (SUHI) under clear-sky conditions, outlining that SUHI is well expressed during the year, while its geometry tends to be more compact and regular during nighttime. In summer daytime SUHI extension reaches its peak, being outlined by the 35°C isotherm, while in winter SUHI is absent during the day. LST increases clearly when imperviousness ratio (IMD) overpasses the 10% threshold, and its maximum is reached for IMD higher than 80%. The comparison with the *in situ* observations indicates that the LST – 2mTair differences are the highest during daytime in spring and summer (+5 to +7°C), while during winter no major differences are observed. For the nighttime the LST is generally 1 to 3°C lower than 2mTair. We also found that intense radiative conditions are prone to increase both the SUHI intensity, and the difference between LST and 2mTair. The results are meant to support the policies aiming to mitigate the heat island effects on human population.

1. Introduction

The Urban Heat Island (UHI) phenomenon, globally extended (Clinton & Gong, 2013; Li, Huang, Li & Wen, 2017, b; Mirzaei, 2015; Peng et al., 2012; Zhou et al., 2017) results basically from the modification of the energy exchange between urban surfaces and the lower troposphere in urban areas that, nowadays, host over 55% of the world's population (United Nations, 2019). This is caused, firstly, by the replacement of evaporative surfaces with impermeable ones and, secondly, by the concentration of anthropogenic heat emissions (Rizwan et al., 2008). UHI contributes to complex changes in regional climate conditions (Shepherd, 2005) with a plethora of environmental impacts, such as vegetation growth (Sfîcă et al., 2018a; Zhao et al., 2016; Zhou et al., 2016) or higher energy consumption (Santamouris et al., 2015). Moreover, these factors affect drastically the biometeorological comfort (Ichim & Sfîcă, 2020) and can lead to an increase in morbidity and mortality (Patz et al., 2005). The effect of UHI and its associated consequences are expected to be increasingly more severe as a result of the

current climate change propagated in a rapidly urbanizing world (Seto et al., 2012). Due to these issues, the UHI has gained considerable research interest and has been the subject of an active investigation, especially in the last decades (Lamb et al., 2019). In this way, UHI became one of the most challenging issue in urban studies which needs to be tackled by diverse strategies and policies proposed in order to mitigate its impact (Mirzaei, 2015; O'Malley et al., 2015).

The definition of the UHI is diverse, but two main types of UHI are of interest to our study. Firstly, the air UHI refers to the effect of the urban area as recorded at the canopy layer (CLUHI) and it is measured by means of *in situ* sensors mounted on fixed weather stations or on vehicles performing mobile measurements (Schwarz et al., 2011; Smoliak et al., 2015). CLUHI analysis could also require special platforms such as tall towers, radiosondes or aircraft (Oke, 2006), but the development of such facilities are time consuming and require considerable financial costs, and therefore they are often available only in large cities (Mirzaei et al., 2010). For this reason, CLUHI analysis does not provide sufficient spatial details for urban planning or climate change research (Anniballe

* Corresponding author.

E-mail address: cretuclaudiu861@yahoo.com (C.-Ş. CREȚU).

et al., 2014; Wang et al., 2017). In general, the CLUHI is weak in late morning and throughout the day, becoming more pronounced after sunset (Sfica et al., 2018a), due to the slow release of heat from urban structures.

Secondly, the surface UHI (SUHI) represents the difference in radiative temperature between urban and non-urban surfaces, being commonly measured using land surface temperature (LST) (Voogt & Oke, 2003). The LST datasets can provide consistent and repeatable observations of the Earth's surface, offering the opportunity to study the urban thermal environment at different spatial and temporal scales (Deilami et al., 2018). They can also be used to predict UHI in a spatially explicit manner (Pichieri et al., 2012). Although, even if it has been assessed from the 1970s (Rao, 1972), publications on SUHI have begun to grow exponentially since 2005, as a consequence of worldwide rapid urbanization during the ongoing climate change, but also due to the progress of remote sensing techniques and processing power, which have improved the quantity and quality of remote sensing data (Zhou et al., 2018).

The SUHI was analyzed for a large number of cities, located especially in Asia (62%), North America (24%) and Europe (15%) (Zhou et al., 2018). It is to be noticed that the studies focused on Europe cover the central and western parts of the continent, in particular, and only few cover the more continental climate of eastern Europe, where Iași city is located. In Romania, SUHI was extensively investigated only for Bucharest (Cheval et al., 2015; Cheval et al., 2009a, b) and Galați (Crețu et al., 2020). A detailed study delivering a country scale image of SUHI for cities in Romania having a population larger than 30000 inhabitants was published recently (Cheval et al., 2022).

As the UHI is usually hampered by the lack of sufficient spatial details, the prediction of air temperature in both urban and rural areas indirectly from satellite observations has gained considerable interest (Fabrizi et al., 2010; Huang et al., 2017; Li, Zhou, Asrar & Zhu, 2018; Pichieri et al., 2012; Sun et al., 2015). Generally, it is observed that the highest CLUHI intensity is observed at night, while the SUHI reaches its peak during the day (Nichol et al., 2009). Overall, it is considered that satellite data largely overestimates the UHI relative to in situ observations (Venter et al., 2021).

In this context, understanding the relationship between SUHI and CLUHI represents a key element for the applicability of LST as a proxy for air temperature (Amani-Beni et al., 2022; Good et al., 2022). This is considered more relevant for climatic studies applied in the field of public health (Venter et al., 2021) or urban design, and consequently more relevant for the studies meant to mitigate the impact of climate change in the cities, a key component of the future sustainable cities. However, finding a simple and general relationship between SUHI and CLUHI is not an easy task (Voogt et al., 2003) and their relationships remains to be better understood. Generally the characteristics of the UHI are controlled by a large number of factors that can be mainly related to local climate conditions manifested under different weather patterns (Reis et al., 2022). While the role of local factors on UHI characteristics is extensively described, the role of weather patterns for the differences between LST (as indicator of SUHI) and screen-level air temperature (as indicator of CLUHI) is worthy of detailed investigation.

To this end, the current study represents one detailed approach focused firstly on the assessment of SUHI for one of the largest cities of Romania, having pronounced features of climatic continentalism at European scale, and secondly on outlining its differences from screen-level air temperature, as indicator of CLUHI. These aspects are further presented taking into account how urban land use and the atmospheric circulation modulate these differences.

2. Data and methodology

2.1. Study region

The Iași urban agglomeration, with over 400,000 inhabitants and

with a dense urban structure in its center, is located in the North-East of Romania (Fig. 1a). The city is developed mainly on the lower terraces of the Bahlui river. The main part of the city is extended at absolute altitudes of 40–80 m and relative altitudes of 10–30 m above the Bahlui river floodplain (Fig. 1b). As observed in previous studies based on in situ measurements (Ichim & Sfica, 2020; Sfica et al., 2018a) the UHI effect is the most pronounced in this area. The city is also developed along the Bahlui River, while in its vicinity six artificial lakes were created after the Second World War (Minea, 2010), both features having the capacity to moderate the UHI as classically known in urban climate studies (Alcoforado & Andrade, 2006), but their impact was not observed in CLUHI characteristics (Sfica et al., 2018a). The climate of the city is temperate, with a high degree of continentalism, the maximum/minimum monthly mean temperature being reached in July (23.4°C)/January (-1.2°C) for the 1981–2020 interval. The annual precipitation amount is moderate (550 mm) with a humid transition between spring and summer and an arid interval overlapping the last part of the summer and the first part of autumn (Fig. 1c).

The city expanded in the 1960s and 1970s in the floodplains of Bahlui river (Roșu & Blăgeanu, 2015). This central area has a high density of built-up space, with limited green urban areas that could reduce the impact of impervious surfaces on the intensity of UHI (Gago et al., 2013). Two types of built-up areas are extended here: residential areas consisting of collective buildings and two large industrial areas (Fig. 1d).

Residential areas, representing the largest part of the city, are located on the hills surrounding its central part, with altitudes reaching 200 m towards the north and 400 m towards the south (Fig. 1c). These hills are oriented from NW to SE (Gugiuman & Cotrău, 1975), representing the dominant exposure of the slope in the city. It is to be noticed that this exposure is a key factor for high insolation during cloudless periods, as those analyzed in our study, leading to amplification of UHI (Sfica et al., 2018a). The high hills on the south of the city (up to 400 m), create a relative altitudinal difference of over 300 m compared to the lowest area of the riverbed. Due to its position, the city of Iași can also be considered a valley city (Utasi et al., 2012), with all the negative consequences derived from this in terms of air pollution (Sfica et al., 2018b).

2.2. Data

2.2.1. Land Surface Temperature (LST) and Normalized Difference Vegetation Index (NDVI)

Sensors placed on board of satellites receive and measure both the reflected shortwave radiation (non-thermal spectral bands) and the long-wave radiation emitted (thermal bands) by the Earth's surface and atmosphere (Mohamed et al., 2017). For SUHI studies, LST data from Landsat (53%), MODIS (25%) and ASTER (7%) sensors are mostly used (Zhou et al., 2018). Moderate Resolution Imaging Spectroradiometer (MODIS) is a key instrument of this type, aboard the Terra (1999) and Aqua (2002) satellites, being launched by NASA to scan the Earth's surface and atmosphere with a 36-band spectrometer, providing global coverage of each day for temperate latitudes (Wan et al., 2001). MODIS records its images at a spatial resolution of 250 m (bands 1–2), 500 m (bands 3–7) and 1 km (bands 8–36). Thus, the great advantage of MODIS imagery is given by its LST high accuracy (Wan et al., 2001), but especially by its temporal resolution, making the LST MODIS a reliable proxy for air temperature (Georgiu & Varnava, 2019).

For the current study, the products MOD11A1 V6 (Terra platform) and MYD11A1 V6 (Aqua platform), each of them with 2 images per day were used, covering the 2003–2020 period, which includes the interval 2013–2020 for which data obtained through data loggers located across the city are available. This interval also includes the interval 2013–2020 for which data obtained through data loggers located across the city are available. We selected LST, quality control (QC) and view time (time at which the image was obtained) for each pixel of the analyzed region and for each observation. More details about these products are presented in

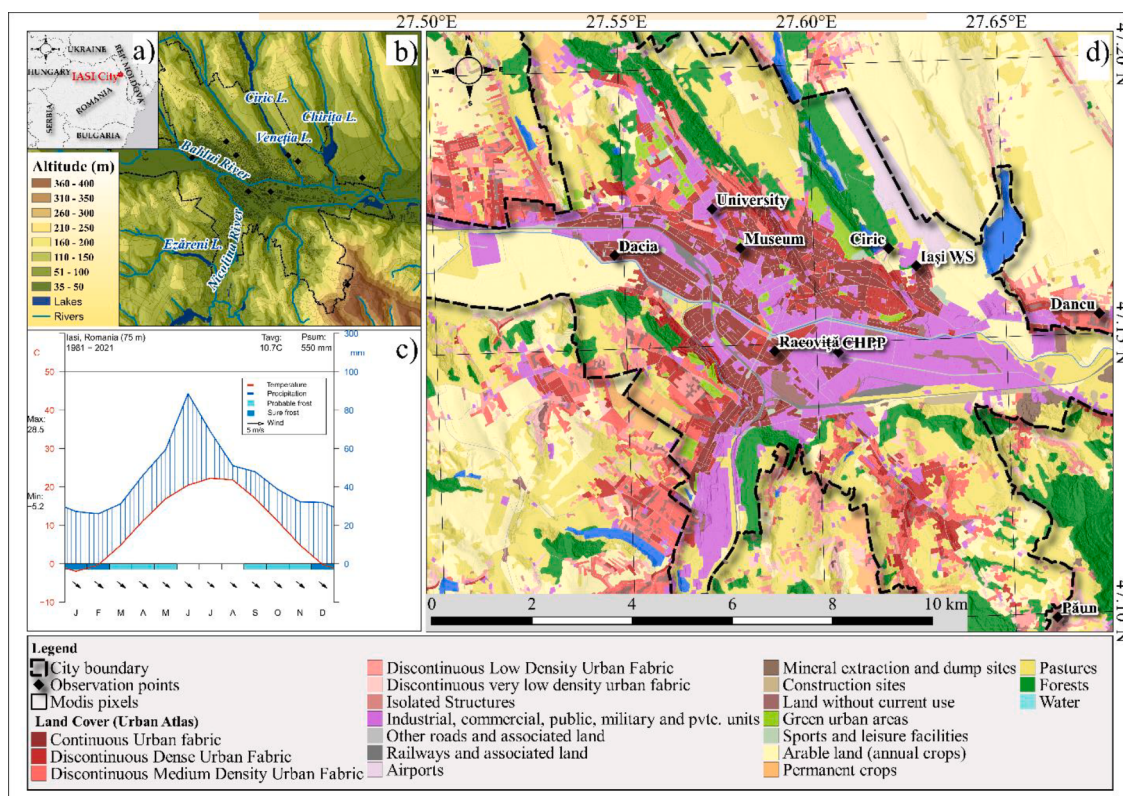


Fig. 1. Geographical position in Romania (a), hypsometric and hydrographic characteristics (b), Walter-Lieth climogram (c) and the main land use categories as derived from Urban Atlas of [Copernicus Land Monitoring Service \(2018a\)](#) for Iasi city (d).

detail in Collection-6 MODIS Land Surface Temperature Products User Guide ([Wan, 2019](#)). These products were obtained through "The Application for Extracting and Exploring Analysis Ready Samples" ([AppEEARS, 2021](#)).

For a detailed look inside the core of the Iași SUHI we also analyzed a set of images from two specific days with typical weather in radiative conditions for winter (10.01.2021) and for summer (14.07.2021). In these case-studies, for each of the analyzed day we have used the MODIS LST image, but also surface reflectance images from Sentinel-2 (having spatial resolution of 10–60 m) and MODIS (having spatial resolution of 250 m) to obtain NDVI products.

2.2.2. Ground network observations for CLUHI assessment

We collected in situ measurements of screen-level air temperature, with an hourly sampling rate, between 1 of January 2013 and 31 of December 2020 in order to compare them with LST. The observations were made with certified sensors for air temperature (HOBO), installed in classical wooden shelters, built after a modified Stevenson screen shelter. The observations were made at a height of 2 m, the shelters being located generally above grass-covered surfaces, according to the specific installation conditions recommended by [Oke \(2006\)](#) in an urban environment ([Sfîica et al., 2018a](#)). Additionally, the data from Iași official weather station were taken from Integrated Surface Database ([NOAA NCEI, 2001](#)).

The 9 monitoring points sample the most important urban land cover categories (Fig. 1d), being installed in representative conditions for the urban structure and its surroundings, as follows:

- Non-urban monitoring points sum up 4 points located in the vicinity of the city: Dancu (59 m), Cîrci (48 m), Iași official weather station (70 m) and Păun (370 m). As specific conditions, Cîrci monitoring point is located in natural conditions in the proximity of a small lake surrounded by forested area, while Dancu monitoring point is

located at the margins of a suburban village. The location and the characteristics of the built up area in their proximity enable us to consider them as being representatives for the area that is not under direct influence of the Iași UHI.

- Urban monitoring points represent the rest of 5 monitoring points whose location was chosen so that they cover the variety of land use categories, in the inner side of the city, as indicated by Urban Atlas. They are located along the river, sampling the highly densified urban residential area built during the communist period (Dacia, 42 m), a green area in the central residential area (Racoviță, 43 m) and the industrial area (CHPP, 40 m). Besides this, one point is located in the oldest part of the city, on the main terrace of the river (Museum, 68 m), while the last one corresponds to University's park (University, 100 m).

Actually, this monitoring network supported the first major assessment of the Iași CLUHI ([Sfîica et al., 2018a](#)), pointing out that the CLUHI reaches annually an intensity of 0.8°C and is more intense during summer nights, when it overpasses 3°C.

2.2.3. Synoptic conditions assessment

Aiming to identify the differences from SUHI and CLUHI determined by regional atmospheric circulation, we used COST-733 software conceived to produce atmospheric circulation classifications ([Philipp et al., 2010, 2016](#)). From all the classification available in this software, we selected the Gross Wetter Typen (GWT) classification ([Beck et al., 2007](#)), describing 18 types of synoptic conditions over a spatial domain having the study region in its center (Fig. 2).

As input data, in this classification software we used Sea Level Pressure (SLP) gridded data from ERA-5 data base. The GWT method calculates the Pearson correlation coefficients between the input data for each timestep and each of the three prototype patterns: zonal, meridional and cyclonic, and uses the combinations between these

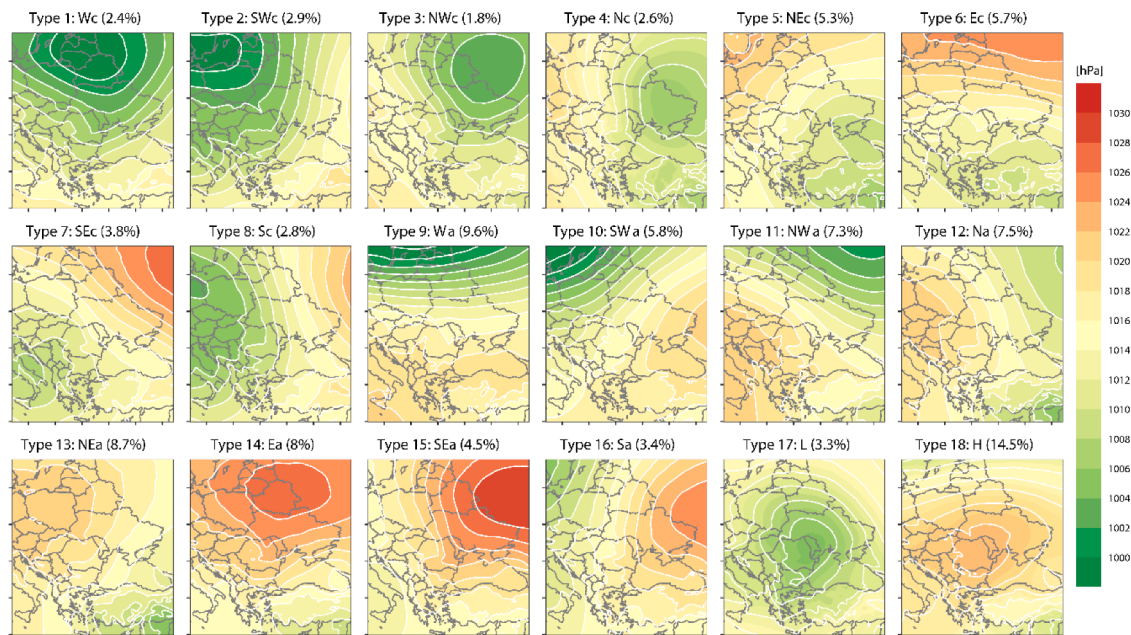


Fig. 2. The distribution of SLP from ERA-5 database for the 18 types of atmospheric circulation as they are indicated by the Gross Wetter Typen classification for 1981–2021 and their annual mean relative frequency (%) over the spatial domain centered on the study region.

coefficients to assign each input field to one class (Beck et al., 2007). Thus, it takes into account the main wind sector and the degree of cyclonicity, resulting in 9 cyclonic types (1–8, 17) and 9 anticyclonic types (9–16, 18).

2.2.4. Other types of data

To spatially represent the urban structure, the imperviousness density (IMD) provided by Copernicus Land Monitoring Service (10×10 m spatial resolution) for 2018 was used in our study (Fig. 3).

IMD captures the percentage of impervious surfaces, indicating the changes in natural soil sealing determined by urbanization through the replacement of the original (semi-) natural terrain or the surface of the water with an artificial, often impermeable coating. The level of the sealed soil (degree of impermeability from 1 to 100%) is produced using a semi-automated classification, based on NDVI from [Copernicus Land Monitoring Service \(2018a\)](#). This also integrates the information regarding built-up area inside the city limits.

The main type of urban land cover (Fig. 1d) were used in the current

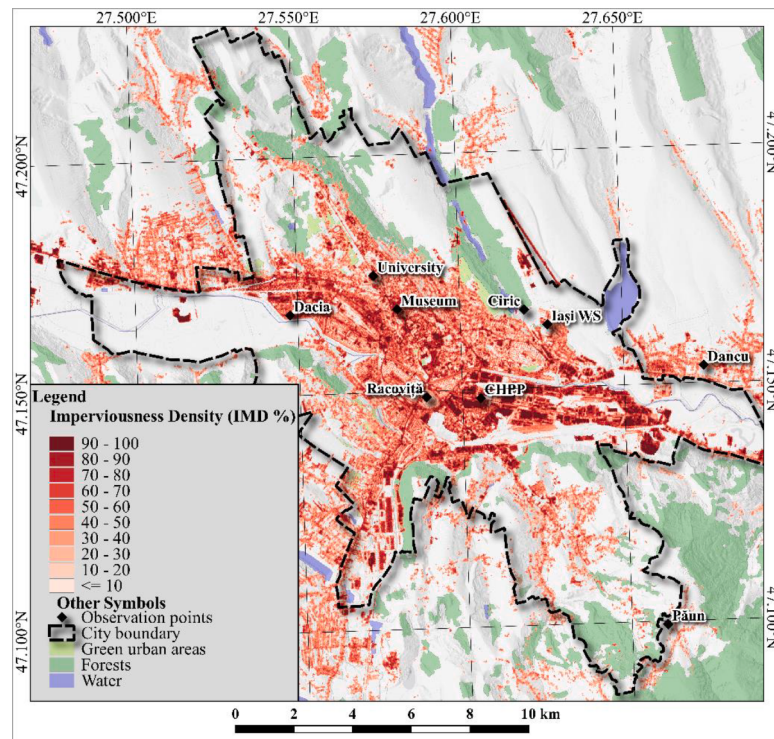


Fig. 3. IMD for Iași city derived from [Copernicus Land Monitoring Service \(2018a\)](#) and the location of in situ monitoring points for air temperature and relative humidity in service between 2013 and 2020.

analysis from Urban Atlas ([Copernicus Land Monitoring Service, 2018b](#)). This land use classification is produced by the European Union regional policy for the production and maintenance of detailed information on land cover.

A synoptic table indicating in details the characteristics of all the types of data used in this study is presented as Supplementary Materials (Table S1).

2.3. Methodology

2.3.1. Selection and treatment of LST data from MODIS satellite images

In order to represent the spatial distribution of the SUHI, the first step was to download all the clear sky satellite images covering the study area from MOD11A1 and MYD11A1 products for 2003–2020. The aforementioned products were extracted in raster format (Geotiff) for an area of approximately 500 km² ([Fig. 2](#)). The resulted dataset was processed using Qgis 3.18.1 tool. Through it, only images with 95.7% valid pixels within the presented polygon were selected, the remaining 4.3% being filled with data by using the r.fillnulls function that covers data gaps.

In this way, the total number of selected images used for this study was reduced to 2901, representing an multi-annual mean of approximately 90 days per year ([Table 1](#)). This largely corresponds with the number of clear sky days per year for the studied region ([Sandu et al., 2008](#)) and, consequently, our study is focused on these kinds of days that are prone to intensify the SUHI due to their intensive radiative processes ([Zhang et al., 2014](#)).

Furthermore, in order to assess SUHI in details, the first step was to apply a 100 m spatial resolution grid whose extension would cover the entire area for which the MODIS products were extracted. On this grid, 2 transects were drawn on the main N-S and W-E directions, as well as 16 buffer zones arranged from 0.5 to 0.5 km, from the city center up to 8 km away of it ([Fig. 4a](#)). The transects show the variation of LST along them, while the buffer zones are meant to show the smoothed tendency of LST as we move away from the city center.

The SUHI intensity is generally quantified in two steps. Firstly, urban and reference areas are defined and delimited through ancillary information. In general, the urban area is delimited by land with a relatively larger portion of impermeable surfaces ([Imhoff et al., 2010; Peng et al., 2012; Peng et al., 2018; Zhou et al., 2017](#)). In this study, the urban area is delimited by IMD ratio higher than 50% ([Fig. 4b](#)).

Recently, [Li et al. \(2018b\)](#) estimated the intensity of the SUHI through the linear regression functions between the SUHI and the Imperviousness Surface Area (ISA). Since ISA is very similar to IMD we applied the method proposed by [Li et al. \(2018b\)](#), but using IMD data. In order to perform the linear regression between LST and IMD data, we brought the IMD data to the same resolution as MODIS LST. To do so, it was necessary to regionalize IMD using a Kernel Density Estimation (KDE) method. During this process, a smoothly curved surface (kernel surface) is mounted on the circular vicinity of each point based on the function of the quartic core ([Silverman, 1986](#)) and from this surface the IMD data with the same resolution as for LST was extracted. The value of the surface is the highest at the place of the point and decreases with increasing distance from that point, reaching zero at the edge of the circular neighbourhood. Subsequently, f_{KDE} was normalized (range from 0 to 100%) using the following formula, similar to how [Li et al. \(2018b\)](#)

proceeded with ISA:

$$IMDKDE = \frac{f_{KDE} - \min(f_{KDE})}{\max(f_{KDE}) - \min(f_{KDE})} * 100$$

To find out the optimal core radius, a sensitivity test was performed by selecting values from 1000 m to 5000 m with a range of 500 m. Thus, LST shows the best relationship with regionalized IMD via KDE, using the core radius of 2500 m ([Fig. 4a](#)). Next, to present the relationship between LST and IMD, linear regression is obtained through the r.regression.line function within QGis.

2.3.2. MODIS-SENTINEL image disaggregation

To give a close up at LST distribution inside the core of Iași SUHI, which is of great interest for specialist in urban design and stakeholders interested in the mitigation of the effect of urban heat island, we present a study case based on satellite fusion method. The fusion methods have been developed to simulate satellite time series with a high spatial and temporal resolution by combining images from two satellites, one that offers low spatial/high temporal resolution, and another one with high spatial/low temporal resolution ([Bisquert et al., 2015; Gao et al., 2006](#)).

For this study, the information in the optical domain (VNIR) from Sentinel-2 is used in the disaggregation of thermal images from the MODIS sensor, aiming to obtain an image of LST with a spatial resolution similar to Sentinel-2. The disaggregation method is based on the linear relationship between the NDVI and the LST on MODIS images. Even if it was originally developed to be applied on images from the same satellite ([Agam et al., 2007](#)), it has been shown that it can be applied for the disaggregation of MODIS thermal images with 1 km spatial resolution to Landsat 60 m spatial resolution ([Bisquert et al., 2016](#)). In this way, we can obtain thermal images with high spatial resolution from the combination of a low spatial resolution MODIS thermal image with a high spatial resolution Sentinel-2 VNIR image, the linear relationship between NDVI and LST leading to best results ([Bisquert et al., 2016](#)). In our study NDVI-LST statistical relationship for MODIS images ([Fig. S1](#)) was stronger for 14th of July 2021 ($R^2=0.81$) than for 10th of January 2021 ($R^2=0.15$). Moreover, the statistical relationship between MODIS and Sentinel-2 NDVI follow the same pattern, with better correlation for 14th of July 2021 ($R^2=0.76$), than for 10th of January 2021 ($R^2=0.09$), indicating that NDVI is a good proxy for the LST only for the analyzed summer day. For this reason, we present in the manuscript only the relevant result for summer day, given that the result for the winter day represents only a poor approximation at high spatial resolution of LST distribution in the center of Iași SUHI ([Fig. S2](#)). The corresponding equations between LST and NDVI for MODIS were applied for Sentinel-2 NDVI to obtain LST with high spatial resolution.

2.3.3. Assignment of LST data to in situ measurements

In order to perform a comparison between SUHI and CLUHI, the first step was to obtain the data from MOD11A1 and MYD11A1 products for 2013–2020, which represents the common period with available data, for each temperature sensor located in the city. The LST and in situ measurements were also selected for the exact time-of-the-day, as recommended in other studies ([Zhang et al., 2014](#)). For this, the hourly data from in situ measurements have been downsampled to the passage time of the MODIS satellite, using the interhourly temperature time gradient,

Table 1

Time intervals of satellite crossing and the number of images selected for Iași city (2003–2020).

Product	Pass time (local)	Jan	Feb	Mar	Apr	May	Jun	Jul	Aug	Sep	Oct	Nov	Dec	Total
MOD11A1 - Day	10:35-13:17	29	25	69	84	74	76	95	137	74	74	40	25	802
MOD11A1 - Night	21:05-00:11	41	37	61	68	59	31	39	81	64	76	31	47	635
MYD11A - Day	13:11-15:05	22	14	66	68	58	68	58	134	80	44	47	22	681
MYD11A1 - Night	00:47-04:23	40	36	71	81	82	64	73	109	87	69	36	35	783
Total		132	112	267	301	273	239	265	461	305	263	154	129	2901

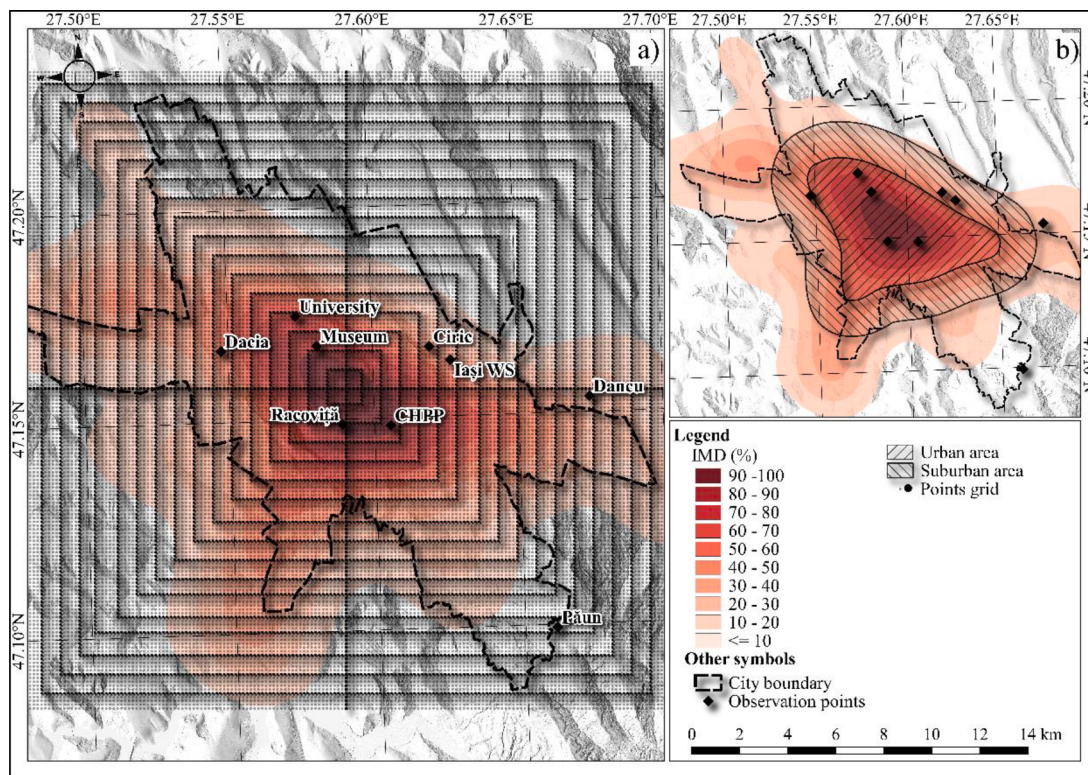


Fig. 4. Buffer areas between 0,5 and 8 km far from the city center (a) and IMD ratio regionalized by Kernel Density Estimation method (b) for Iași city.

assuming the linear evolution of air temperature.

Using AppEEARS, daily per-pixel LST with 1 km spatial resolution was extracted for each in situ observation point according to their geographical coordinates, in order to compare the difference between them. In total, for all of the 9 in situ observation points, 10778 MOD11A1-day, 9052 MOD11A1-night, 10850 MYD11A1-day, and 10439 MYD11A1-night observations were selected.

2.3.4. Analysis of differences between SUHI and CLUHI in relation with atmospheric circulation

In GWT classification, used in this study, the synoptic types from 1 to 8 represent cyclonic advective conditions, while the types 9 to 16 impose anticyclonic advective conditions over the study region. Additionally, one type describes pure cyclonic conditions (17), and the last one (18) indicates pure advective conditions dominated by radiative processes (Fig. 2).

The classification used input data for 1979-2021, but we used the results for 2013-2020 which represents the common period with observational data for SUHI and CLUHI. In this classification each day is assigned to one of these 18 weather types depending on the distribution of SLP at regional scale. For the region of Romania, the anticyclonic conditions prevail throughout the year (Niță et al., 2022), as can be seen from our results as well. The anticyclonic circulation types (9-16 and 18) sum up, in a multiannual mean, 73% of the days in a year.

The clear sky days for which the MODIS images were selected are in direct relation with these anticyclonic conditions. From 90.3 available images per year (24.7%), 78.1 of them correspond with these anticyclonic conditions and only 13.4 days are assigned to GWT cyclonic conditions. From all the images in anticyclonic conditions, the major part was characterized by advection conditions dominated by north-eastern (14), northern (13) and western (9) flows on the ground. Also, pronounced radiative conditions (18) were specific for MODIS images in 20.2 days per year. Overall, the MODIS images used in the current study represent 11.9% of the total days characterized in GWT atmospheric circulation with cyclonic conditions, but 30.4% of the days with

anticyclonic conditions (Fig. 5). Thus, it is obvious that our analysis is more representative for anticyclonic conditions than for cyclonic ones. However, it is worth mentioning that anticyclonic conditions are recognized as the most important for contouring the main features of the SUHI.

3. Results and discussions

3.1. Surface Urban Heat Island of Iași

3.1.1. Seasonal characteristics of Iași SUHI and specific land use dependencies

In order to portray the general dynamic of SUHI our analysis is focused both on day and night, and also on the seasonal levels. Generally, Iași SUHI presents, similarly to other cities (Wang et al., 2015), a great diurnal variability embedded in the seasonal variability manifested throughout the year, with an annual SUHI dynamic that indicates the so-called single-peak type, with a maximum in summer and a minimum in winter, as typical for warm temperate and snow climate (Liu et al., 2022).

During winter, especially during the daytime (Fig. 6a), the intensity of SUHI is very low. The maximum average LST is located over the city center and reaches +5.0 °C during the day and -4.0 °C during the night. The limits and geometry of SUHI during the day are difficult to be assessed and the maximum LST is observed over the city, but also over the terrain slopes exposed to the south. During the night instead, Iași SUHI reaches 1.5 °C in intensity (Fig. 6b), laying its center over a region outlined by the isotherm of -4.0 °C.

The spatial extention of SUHI is influenced in winter mainly by the local topography that enhances frequent developments of thermal inversions and induces differential radiative heating between the northern and the southern terrain slopes. At this time of year, the frequency of thermal inversions was estimated by Ichim et al. (2014) at about 30% of the time at hourly level, these thermal stratifications being characteristic mainly for anticyclonic conditions. Thermal inversions cause a drop in

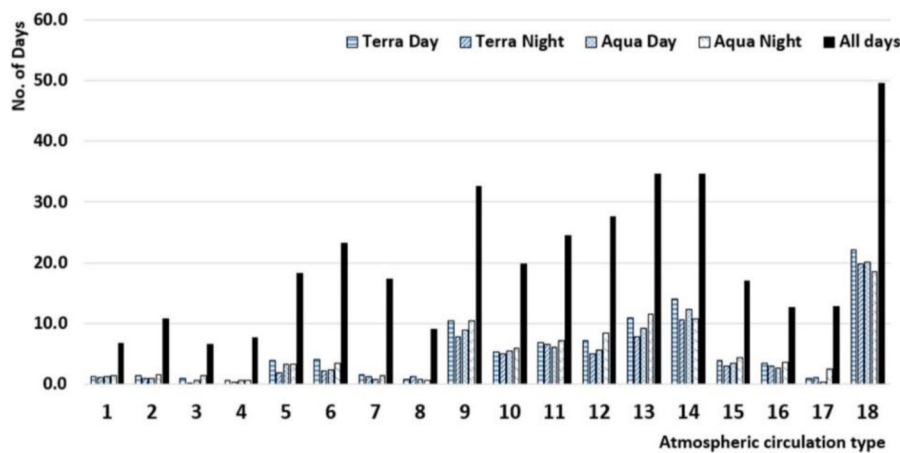


Fig. 5. Absolute frequency (no. of days per year) of 18 types of atmospheric circulation according to GWT method and the distribution of available MODIS clear sky images used in the current study per each atmospheric circulation type (2013-2020).

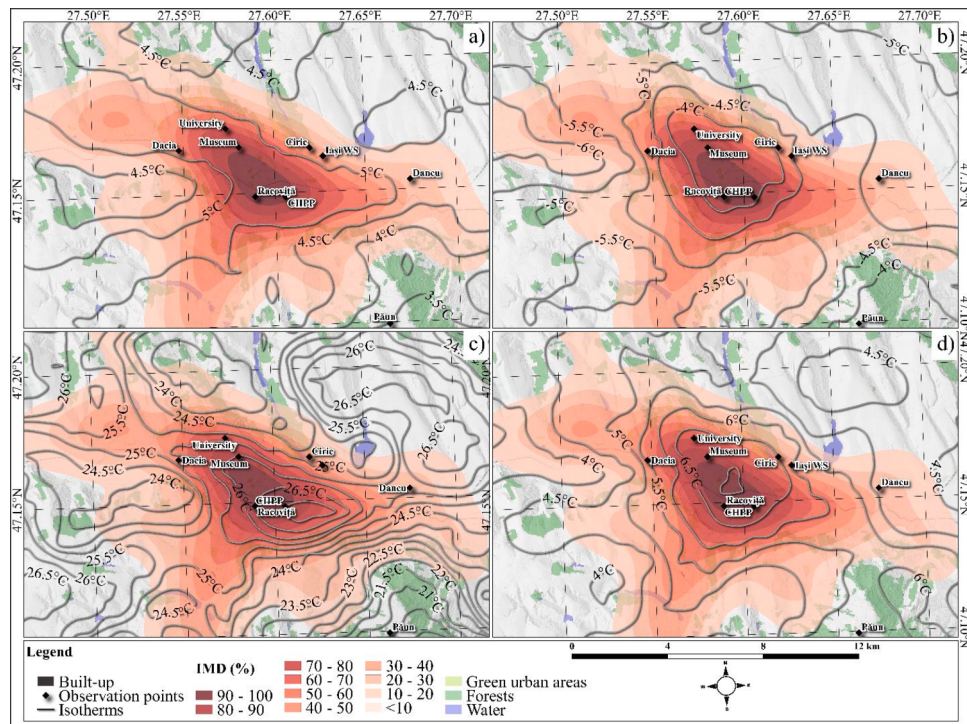


Fig. 6. Distribution of mean LST during winter day (a), winter night (b) spring day (c) and spring night (d) over Iași city derived from MODIS imagery (2003-2020).

air temperature along the floodplain of the Bahlui river, inducing, at least apparently, a lack of SUHI. In fact, the thermal effects of SUHI during the winter nights are canceling the cooling effect of night thermal inversion and consequently we can observe that the air temperature over the highest hills in the south-east of the study region are the same with those contouring the city center (-4.0°C). It is worth mentioning that, the weaker winter SUHI is in direct relation with a weak winter CLUHI, as observed by Sfica et al. (2018a).

During the spring daytime (Fig. 6c), SUHI has a low intensity and extension, covering almost half of the total built-up area. Moreover, the extension of SUHI over the industrial area of the city, located along the river valley, is better expressed during the day, while during the night the warmest core extends more towards the old part of the city located on the river terraces. During the day the influence of the thermal inversions vanishes so that the core of SUHI ($>27.0^{\circ}\text{C}$) covers the industrial region having an intensity of $+1.0\text{-}1.5^{\circ}\text{C}$. Also, the effect of SUHI

overpasses the thermal radiative effect on the arable lands from the north-east, north-west and south-east of the city ($26.0\text{-}26.5^{\circ}\text{C}$). During the night, however (Fig. 6d), the thermal inversions bring high LST values in south-eastern upper region, while the river valley located at the western part of the city and the arable lands in north-east record the lowest LST. In this interval SUHI is clearly expressed, with its warmest core right over the city center, being delimited by the 7.0°C isotherm. This represents an intensity of $2.5\text{-}3.0^{\circ}\text{C}$ compared to LST along the river valley in non-urban areas. These features of SUHI are in correspondence with CLUHI that is well contoured, but not very intense during spring (Sfica et al., 2018a).

Furthermore, SUHI shows the highest intensity during the summer (Fig. 7a, 7b), while during the autumn (Fig. 7c, 7d) it shows similar values to those observed during spring.

Actually, SUHI expansion reaches its peak during the summer season due to the higher frequency of radiative conditions associated with

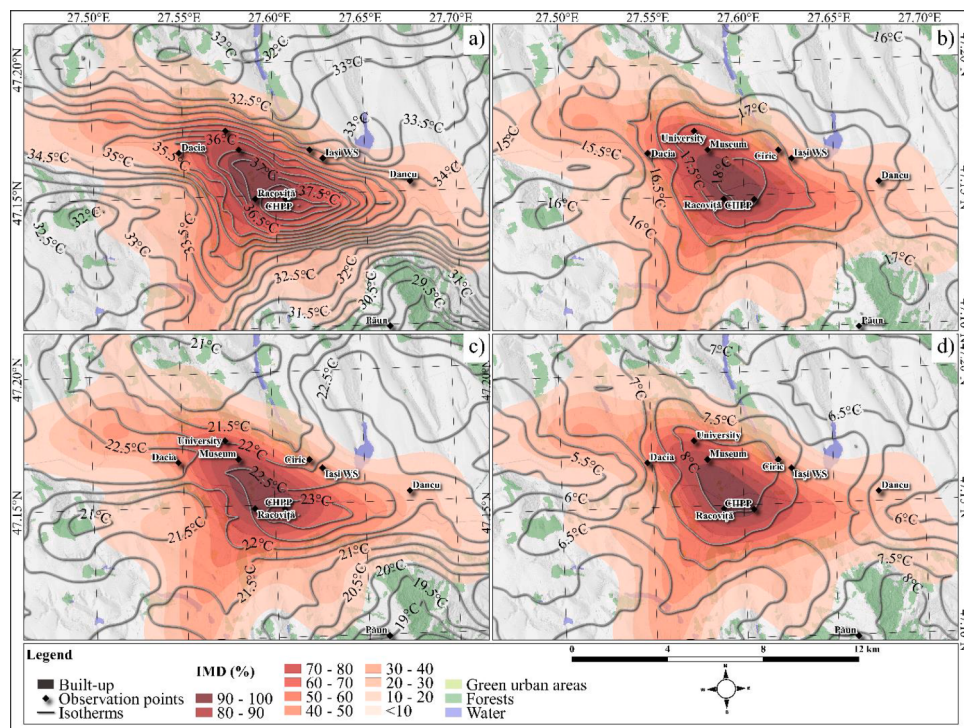


Fig. 7. Distribution of mean LST during summer day (a), summer night (b), autumn day (c) and autumn night (d) over Iași city derived from MODIS imagery (2003–2020).

intense insolation and low cloud cover, which are generally known to lead to an increase in UHI intensity (Shachgedanova et al., 1997). The SUHI reaches its highest intensity with LST mean values over 38°C in the same region as in spring. We notice that SUHI is extended over the industrial area of the city and over its central part, in direct relation to the densely built-up area.

Also, the SUHI intensity increases to +3.0–3.5°C during this time being very steep towards the hilly area north and south of it. The maximum SUHI intensity instead, during summer day contrasts with the observed feature of CLUHI in the same time interval that describes even slightly colder conditions inside the city (Sfica et al., 2018a) and confirms the strong SUHI in temperate and continental regions (Zhou et al.,

2013), specific for July and August (Sismanidis et al., 2022). This is in line also with the observed higher intensity of SUHI during summer in colder climates of Romania, as is the case of Iași (Cheval et al., 2022).

The intense SUHI could also be enhanced by the large extension of croplands around the city, as recently suggested worldwide (Chen et al., 2021). During the summer nights the SUHI intensity values are slightly lower and keeps the main shape from spring nights. The Iași SUHI peaks 18.0°C and an intensity of 2.5–3.0°C, in direct relation with the peak of annual CLUHI along the year (Sfica et al., 2018a) and could be seen as a consequence of high temperature during summer days as observed by de Ridder et al. (2017).

Due to the complexity of summer day SUHI, we present as a study

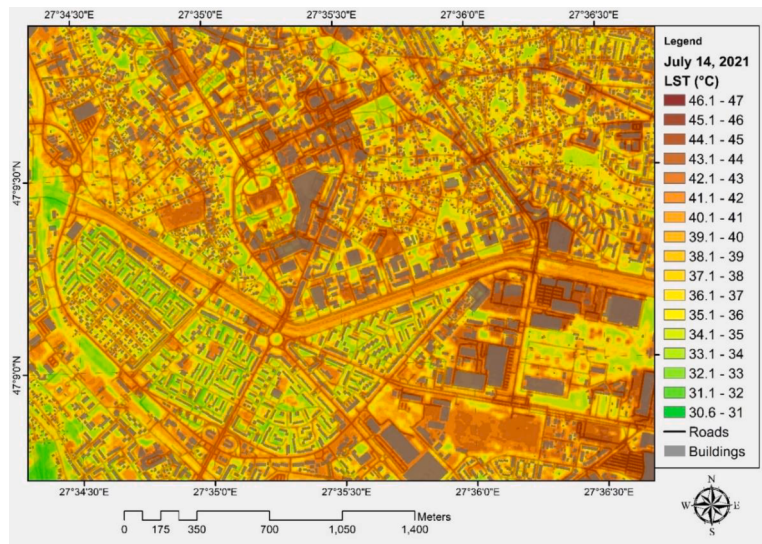


Fig. 8. LST distribution for 14.07.2021 during daytime based on SENTINEL-MODIS NDVI disgregation for the central area of Iași city corresponding with the core of Iași SUHI.

case the distribution of LST for 14th of July 2021, a hot summer day with a daily maximum air temperature of 33.3°C at the official weather station. The high spatial resolution of LST obtained through image fusion indicate a LST range between 30.6°C over the green areas and 47.0°C over the densely built areas of the city (Fig. 8). We can also observe that the larger the green area between collective buildings, the lower the LST of that area, especially for residential areas over the central-southeastern part of the city. This indicates that residential areas dominated by massive collective buildings with very large green areas between them are preferable for the reduction of LST to smaller collective buildings separated by smaller green surfaces.

This case-study synthesizes the LST distribution in a common summer day and could be of great interest for specialists in urban design and stakeholders interested in the mitigation of the effect of urban heat island.

We underline here that we do not stress to much on the CLUHI or SUHI intensities in our study, since we consider this discussion to be largely overrated in climate urban studies. We assessed only empirically the intensity as the difference in mean LST in the warmest core of SUHI and the rural regions with approximatively the same altitude along the river valley of Bahlui river. Due to this specific choice in assessing SUHI, the SUHI intensities presented in our study are higher than those obtained by Cheval et al. (2022).

The imprint of thermal inversions still exists during the summer, leading to an uniformization of air temperature with altitude (16.0–17.0°C).

During autumn, especially during the day (Fig. 7c), the intensity of SUHI decreases to 0.5–1.0°C, but preserves the spring-summer form. During autumn nights (Fig. 7d) the SUHI intensity increases to 2.0–2.5°C, cancelling the thermal effect induced by thermal inversions, as indicated by the similar LST over the city center, but also over the higher

ground in south-east (8°C). The LST values in the core of the SUHI are higher in autumn than in spring, but this is explained more by a higher number of images available from the commonly warmer September, while in October and November the stratiform cloudiness specific for the region decreases the number of available images.

The seasonal SUHI is in a direct relation with IMD ratio, which is the most important contributor to LST variability in temperate climate (Naserikia et al., 2022). This is observed in Iași clearly when we analyze the north to south and west to east LST profiles besides the IMD ratio (Fig. 9).

The north-south profile outlines better the SUHI, but this is enhanced also by the lower LST values specific for the higher ground on the north and south of the city center. The west-east profile instead underlines better the intensity of the SUHI since the hypsometric differences along the transect are very small.

Thus, it can be seen that the SUHI is present in all seasons during the night, while during the day the maximum is reached in summer. In spring and in autumn its intensity is weak, while in winter the SUHI is in place only during the night. Overall, the increase in LST is specific for the points with IMD higher than 10% and reaches its maximum for the area with IMD higher than 80%, especially for the warm season when the relationship between LST and built-up ratio is known to be stronger than in winter (Naserikia et al., 2022). In fact, it was previously assessed that, for Iași city, LST increases during spring and summer with 0.3–0.6°C for each increase of IMD by 10% (Crețu et al., 2022).

3.1.2. Influence of IMD and urban land cover types on LST

The LST averaged for 0.5 km buffer zones, from the city center to the periphery, enables the delimitation of the SUHI core, defined here as the sharpest inter buffer zone LST difference, but also of the SUHI outer limits, defined as the inter buffer zone with no LST difference.

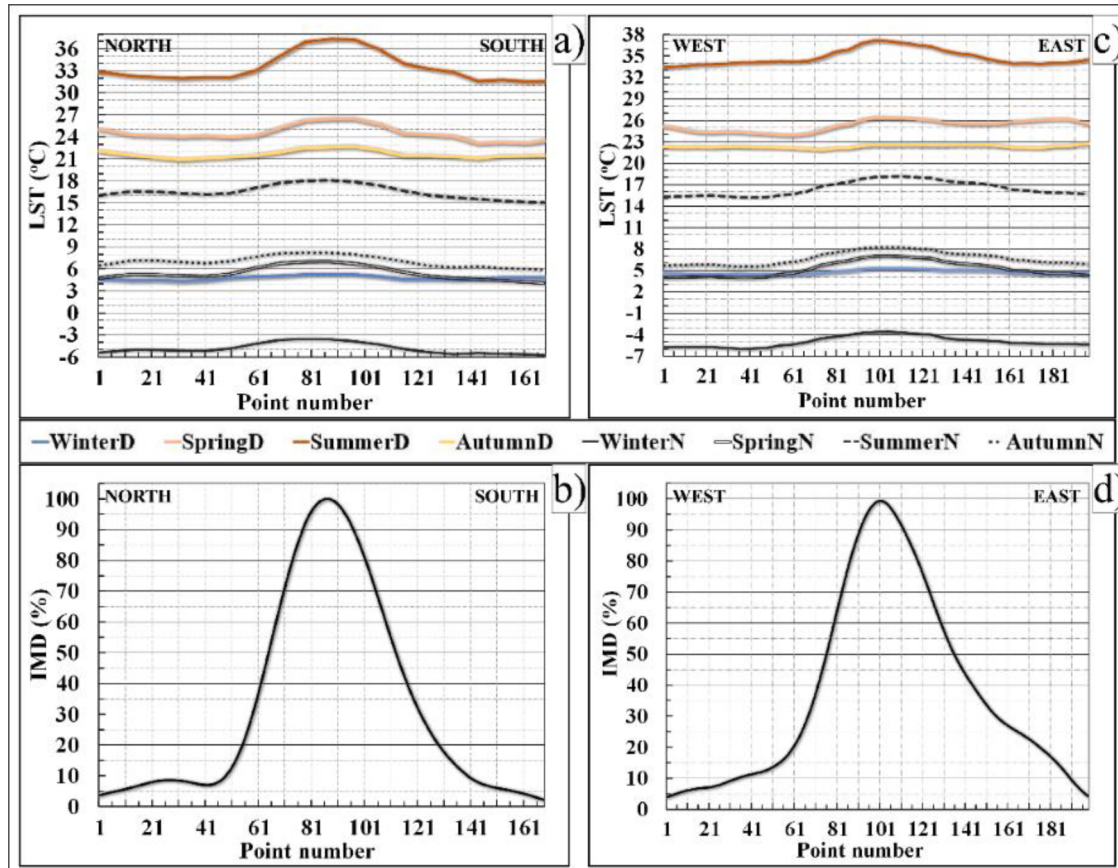


Fig. 9. North-South (a) and West-East (b) LST profiles and their corresponding IMD ratio (c, d) over Iași city as derived from MODIS imagery (2003–2020).

This way, for the day time (Fig. 10a), the core of SUHI extends to 3.5–4.0 km buffer zone around city center in summer and spring, while in autumn and winter SUHI's core is not well outlined. The outer limit of the SUHI instead is located at the level of 5 km buffer zone. For the nighttime instead (Fig. 10b), the core of SUHI is located at 3.0 km buffer zone, while its outer limit is placed at 5 km buffer zone, being clearer in summer. Generally, we can see that these limits correspond to the sharpest increase/decrease of the IMD ratio which is located between 2.5 and 5 km.

The influence of the IMD on SUHI is easily visible on the LST extracted for each urban land use category. The highest LST values are by far specific for continuous urban fabric, both during the day (Fig. 11a) and night (Fig. 11b) throughout all seasons, confirming the role of built-up areas density in increasing LST values in urban environments (Wang et al., 2022).

In summer day, as reflected by the 14th of July 2021 case-study (Fig. 11c), these land use categories records maximum LST value over 44°C. Only during autumn days is the LST maximum on another type of land cover (industrial areas), but with similar IMD characteristics. The lowest mean LST is recorded during the day over forested and green areas, regardless of season. Actually, as known in literature (Good et al., 2022), the category of forested areas records the closest LST values to those recorded at screen-level air temperature.

This proves the cooling effect of forested/green areas, but could also represent an effect of the higher altitude of the forests in the region of Iași. During nighttime the lowest LST values are common for arable lands in all seasons, as a result of the intensive radiative loss during night on this kind of surfaces.

In spring and summer, during the day, the effect of the largest lake in the region is very clear, the LST over these surfaces being 1.2–3.0°C below the core of SUHI, but the local thermal effect is hardly distinguishable due to the low spatial resolution of MODIS images.

3.2. Differences between LST and screen-level air temperature in Iași city

3.2.1. Seasonal characteristics

The difference between LST and screen-level air temperature is very diverse during the day throughout seasons in relation to the annual variation of the global solar radiation, and also with a remarkable effect of urban land use.

During winter days (Fig. 12a) the analyzed differences are close to 0°C, even if we considered to analyse only clear-sky days, this being in line with other studies (Good, 2016; Good et al., 2022). This shows that the radiative warming is weak, which is reflected also in the weak winter SUHI. Moreover, in many situations the LST is close to -20°C lower, especially during the night, than the screen-level temperature, a situation that could be determined by the intense thermal stratification in the lowest troposphere, LST being represented in these cases by the trees

canopy. A similar situation can be found in autumn (Fig. 12d) for the observation points located in the lower (Dacia), rural (Dancu) or green area (University) of the city.

It is worth mentioning that Păun monitoring point, which indicates in all seasons screen-level values closer to LST (Fig. 12a-d), is located in the rural hilly area at an altitude of 370 m, being surrounded by forests and other types of green areas. In this way, the mean difference between day and night is close to 0°C in spring, summer and autumn, and slightly negative in winter. This indicates that for natural areas MODIS LST values represent a reliable proxy for screen-level air temperature at daily level for areas with natural land cover. During summer the difference is smaller for all the points located in semi-urban areas (Păun, Iași weather station and Dancu) or near water body (Ciric). For the other urban observation points, LST is higher with 5–8°C than the 2 m air temperature during the day in spring and summer, and with 2–5°C during autumn, which is in line with other findings proving that SUHI is generally stronger than CLUHI during the day (Azevedo et al., 2016). The differences observed for the summer and spring are also very close to those observed in other studies between clear-sky LST derived from MODIS images and all-sky LST derived from in situ measurements (Gallo & Krishnan, 2022), a similarity that could indicate once more the reliability of using MODIS LST as proxy for screen-level air temperature. During summer, when the insolation is very high the differences between LST and 2 m air temperature can reach even 20°C (Fig. 12c), confirming also previous analysis (Good, 2016).

During nighttime, the differences between LST and the air temperature at 2 m are negative (Fig. 12), but smaller than for the day, as assessed in other studies (Shen et al., 2011). The screen-level air temperatures for the night are generally from 1 to 3°C colder than the emissive surface. The differences are even smaller for Ciric monitoring point due to its position in the near vicinity of a body of water surrounded by forested area, which are characterized by higher temperatures than the neighbouring areas. As a general rule, we can observe that the LST is lower than the screen-level air temperature for the observation points having a higher build-up and impervious ratio, as a consequence of their higher radiative loss during the night.

These results prove mainly that the thermal information given by MODIS satellite images is highly valuable as an indicator of screen-level temperature conditions even in urban areas. However, this information should be used with caution since in a significant number of cases outliers values indicate LST temperature colder with up to 5°C than 2m air temperature in all seasons, most probably due to the influence of high aerosols concentration (Shen et al., 2011).

3.2.2. Differences between LST and screen-level air temperature and their relation with atmospheric circulation

For a detailed and synthesized image of the differences between SUHI and CLUHI we have analyzed them in their relation with atmospheric

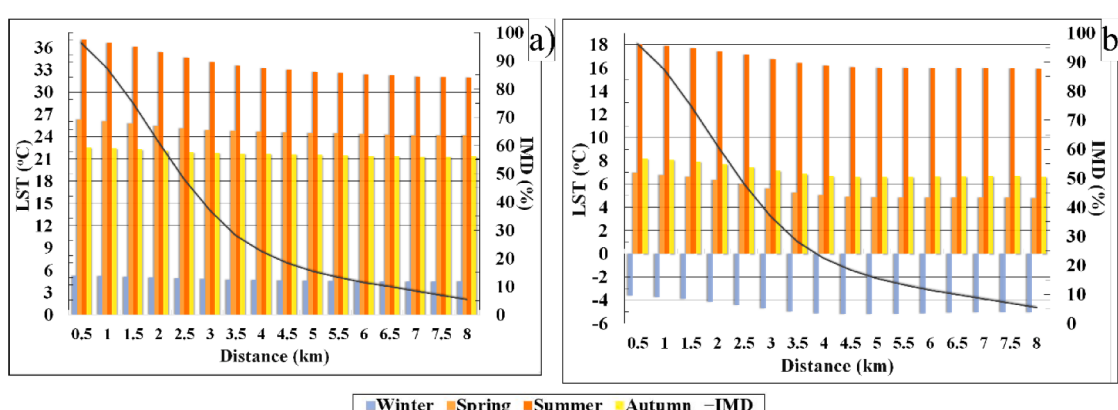


Fig. 10. Distribution of LST for each 0.5 km buffer zones around the Iași (2003-2020) city center for day (a) and night (b) and the associated IMD ratio (%).

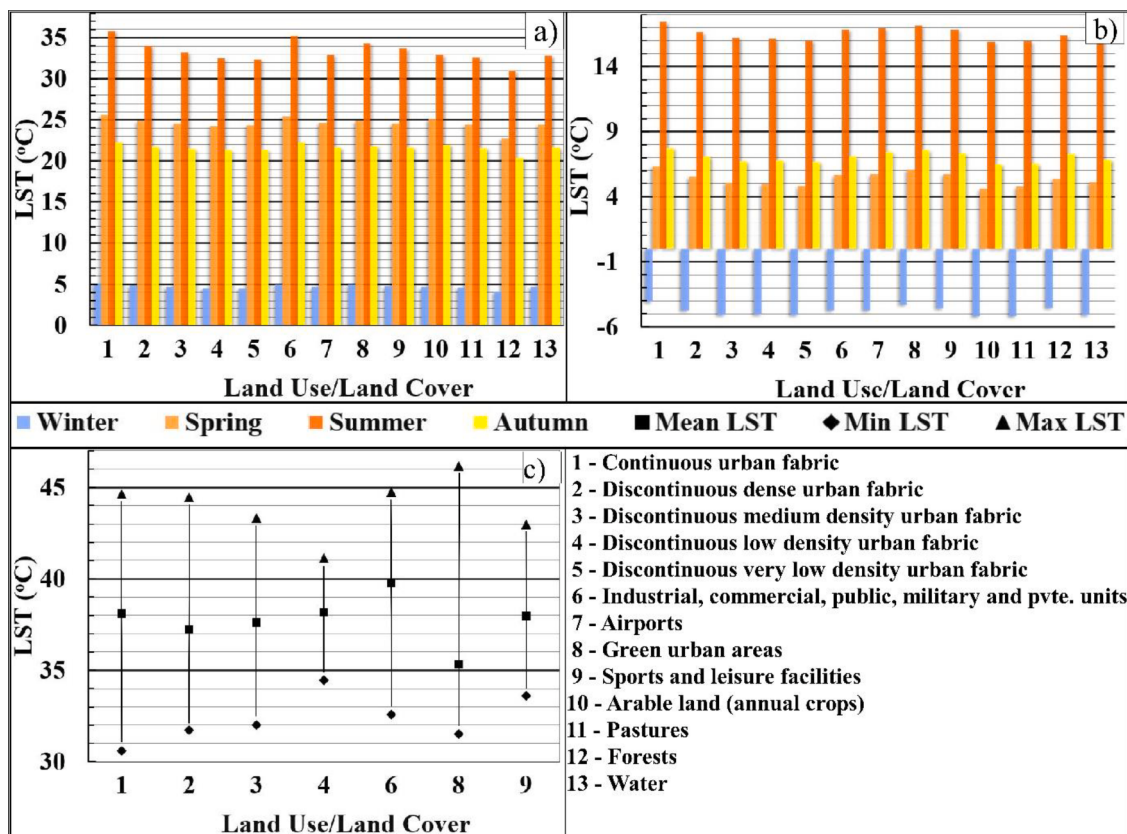


Fig. 11. Mean LST for the Urban Atlas main categories of land use in Iași city for day (a) and night (b) for 2003-2020 and the minimum and maximum LST for the land use categories in the central area of Iași SUHI for 14.07.2021 (c).

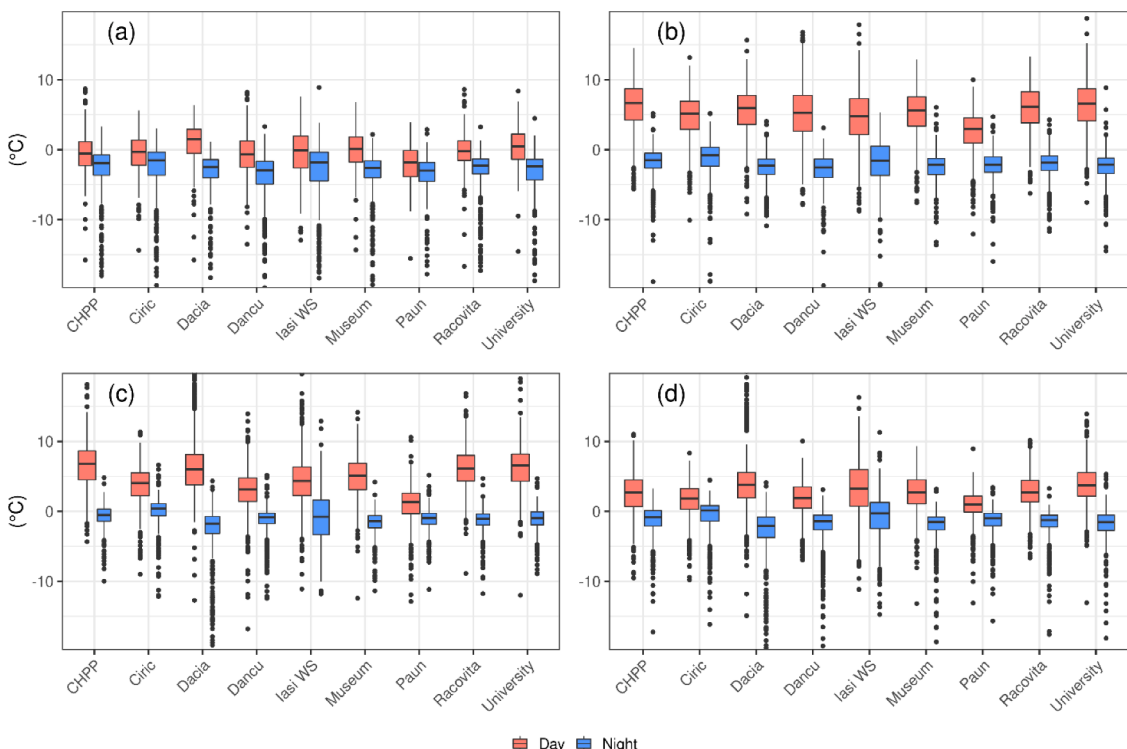


Fig. 12. Difference ($^{\circ}\text{C}$) between LST and screen-level air temperature measured in the 9 monitoring points distributed in selected relevant land use areas in the Iași city during the day and night (2013-2020) for winter (a), spring (b), summer (c) and autumn (d).

circulation. The atmospheric circulation patterns were grouped in 3 main circulation types: cyclonic (GWT types 1 to 8 and 18), advective anticyclonic (GWT types 9-16) and radiative anticyclonic (GWT type 18).

Even if each of these major weather patterns have in common the lack of clouds during the satellite passage, the differences between them from a meteorological point of view, as reflected by mean daily relative humidity (Fig. 13a), daily precipitation amount (Fig. 13b), mean wind speed (Fig. 13c) and mean solar radiation (Fig. 13d) are not negligible, and can explain partially the nature of the differences between LST and screen-level air temperature.

Firstly, we observe that the solar radiation amount is similar in all the 3 major weather patterns, because of the analysis restricted to cloud free days. The cyclonic weather pattern is characterized by a higher relative humidity and even precipitation amount, obviously occurred before or after the satellite passages, while the radiative anticyclonic conditions are characterized by the lowest wind speed and relative humidity, which most probably represent a key for more intense radiative fluxes leading to higher differences between LST and screen-level air temperature.

In addition, the 9 monitoring points were grouped in 3 main classes depending on their morphographic features and land use: high rural (represented only by Păun mp), low rural (represented by Cîrcic, Dancu and the official weather station) and urban (Dacia, University, Museum, Racoviță and CHPP mps).

The results of this clustering are presented for annual level during the day in Fig. 14a and for cold and warm season in Table 2, while for the night in Fig. 14b and for cold and warm season in Table 3.

At annual and seasonal levels, during the day, the differences are in direct relation with major land use categories, but more loose between the major weather patterns. In brief, the differences are increasing from high rural to urban land use during the day (Fig. 14a), in correspondence with the radiative heating related to built up areas, and are slightly higher for radiative anticyclonic conditions than for cyclonic or advective anticyclonic conditions, mostly due to higher insolation and slow wind speed (Fig. 13c), as observed in other studies (Good et al., 2022).

During the night, the differences are overall negative (Fig. 14b), with no significant differences between major weather patterns or land use

categories. However, due to the higher IMD ratio, the urban areas record the highest negative differences between LST and screen-level air temperature. During the night, the radiative loss is more intense, but these conditions are more pronounced for cyclonic conditions in rural area. This could be explained by the higher fresh snow ratio leading to more intense radiative cooling in rural areas that records a more important snow-pack than urban areas (Sfica et al., 2018).

An explanation for these observed high differences between LST and screen-level air temperature resides from the fact that LST is explained more by land cover terrain and city morphology (Venter et al., 2021), while screen-level air temperature is more complex, being under the influence of many parameters (Amani-Beni et al., 2022). Among these factors, our study indicates the important role of atmospheric circulation. Not to forget as well, that the cyclonic conditions with clear sky are not very frequent so that for the contouring of the SUHI the impact of anticyclonic conditions, both advective, but especially radiative, is by far the most important.

4. Conclusions

The increasing accessibility to high resolution LST data unbalances recently the investigation of the UHI towards approaches based on these remote sensing tools. However, for a holistic assessment of UHI, a need to compare the resulted surface UHI with the canopy layer UHI remains of great interest. In our study, we responded to this demand by taking into account all the MODIS LST images and their corresponding synchronous air temperature observations from 9 in situ monitoring points evenly distributed over the city of Iași for 2013-2020.

This way, using a total of 2901 satellite images, the main diurnal and seasonal characteristics of clear-sky SUHI have been outlined for Iași city. The results obtained describe accurately the intensity of the SUHI, but also its relation with the urban land use categories. During daytime, in summer season the spatial extent of SUHI reaches its maximum, SUHI being bounded by the 35°C isotherm and peaking 38°C in its center, in direct relation with the highest imperviousness density. In the winter season, SUHI is almost absent during the day, especially due to the high frequency of thermal inversions over the study area. The geometry of

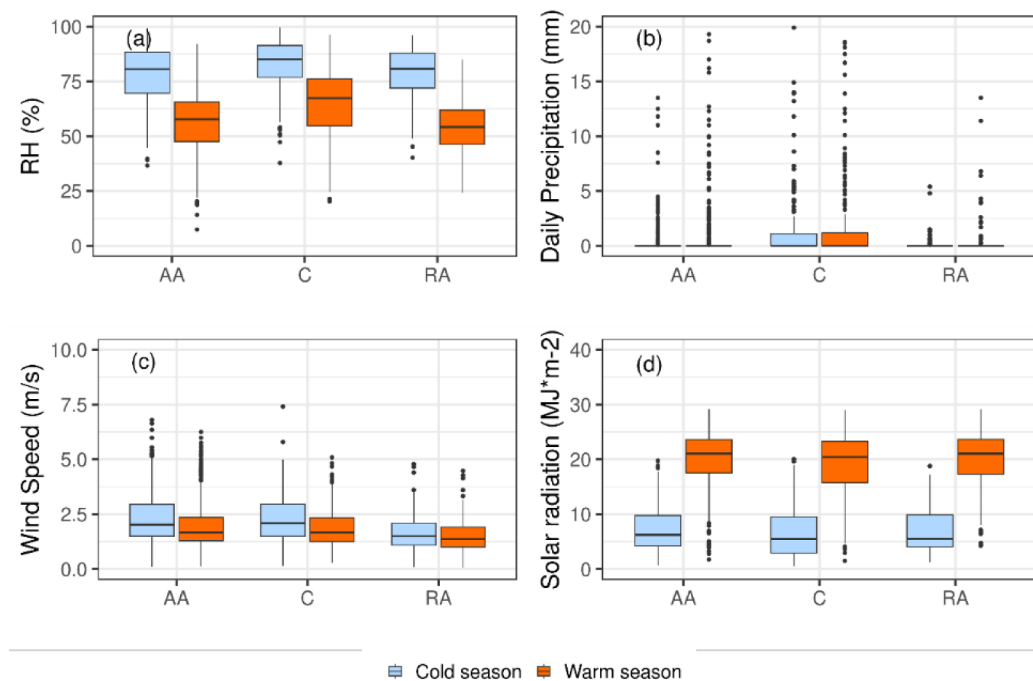


Fig. 13. Specific weather conditions indicated through mean relative humidity (a), daily precipitation amount (b), wind speed (c) and solar radiation (d) for the main types of atmospheric circulation (anticyclonic advective, cyclonic and radiative anticyclonic) for Iași city (2013-2020).

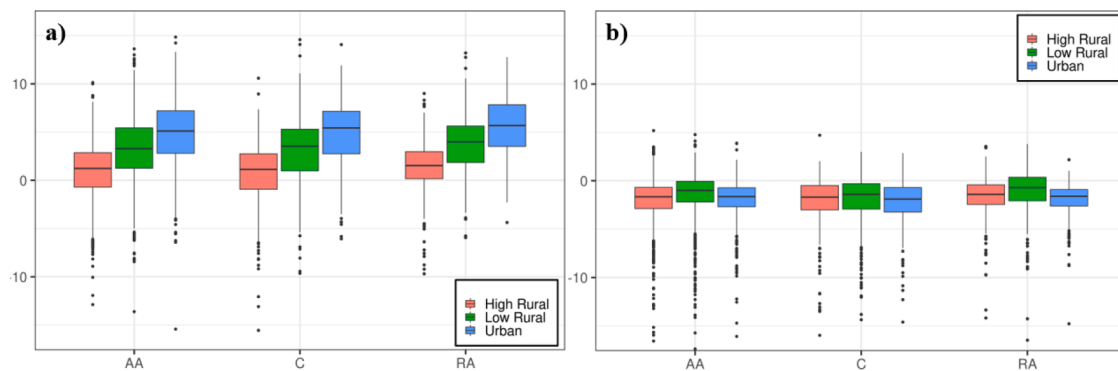


Fig. 14. Difference ($^{\circ}\text{C}$) between LST and screen-level temperature for the main type of monitoring points (high rural, low rural, urban) and for the main types of atmospheric circulation (anticyclonic advective, cyclonic and radiative anticyclonic) for Iasi city during day (a) and night (b) for 2013-2020.

Table 2

Difference ($^{\circ}\text{C}$) between LST and screen-level air temperature for major groups of weather patterns (cyclonic, advective anticyclonic and radiative anticyclonic) and for major land use categories (high rural - HR, low rural – LR and urban - U), during the day for Iasi city (2013-2020).

	Cyclonic			Advective anticyclonic			Radiative anticyclonic		
	HR	LR	U	HR	LR	U	HR	LR	U
Year	+0.8	+3.2	+4.8	+1.0	+3.3	+4.9	+1.5	+3.9	+5.7
Warm season	+1.2	+4.1	+5.9	+1.5	+4.3	+6.2	+1.8	+4.5	+6.6
Cold season	-0.5	+0.9	+1.8	-0.1	+1.3	+2.1	+0.9	+2.5	+3.3

Table 3

Difference ($^{\circ}\text{C}$) between LST and screen-level air temperature for major groups of weather patterns (cyclonic, advective anticyclonic and radiative anticyclonic) and for major land use categories (high rural - HR, low rural – LR and urban - U) during the night for Iasi city (2013-2020).

	Cyclonic			Advective anticyclonic			Radiative anticyclonic		
	HR	LR	U	HR	LR	U	HR	LR	U
Year	-2.1	-2.1	-2.3	-2.0	-1.4	-1.9	-1.6	-1.1	-1.9
Warm season	-1.5	-1.3	-1.7	-1.4	-0.9	-1.5	-1.0	-0.7	-1.6
Cold season	-3.3	-3.3	-3.0	-2.9	-2.1	-2.4	-2.4	-1.6	-2.2

SUHI tends to be more compact and regular during nighttime and more irregular during daytime, as a result of the higher and more complex energy input.

The comparison with the screen-level in situ observations indicates that the differences from LST are highest during daytime in spring and summer, when LST is 5 to 7°C higher than the screen-level air temperature, while during winter no major difference can be observed. For nighttime the LST is 1 to 3°C lower than air conditions regardless of seasons, as an effect of the radiative loss at the surface. This analysis proves that the LST derived from MODIS satellite images could be used even in urban areas, with high confidence, to downscale screen-level air temperature, a temperature parameter which is more relevant for applied studies, especially during the night.

The study's results could help to better understand the relation between LST and in situ observations in urban environments, which is useful for the assessment of thermal comfort, the main target of the policies oriented towards the mitigation of urban heat island effects in the context of the current climate change.

Overall, we consider that our study contributes to the filling of this knowledge gap in the field of SUHI that affects the general understanding of the urban heat island phenomenon for medium sized cities in Eastern Europe and present a pronounced scientific interest for those regions that shift in the current climate change from D-type towards C-type of climate in Köppen climate classification. In this context, our results should be regarded as being specific only for this type of regions and that the extrapolation of our results to larger scales should be made

with caution.

The results of this study are planned to be reinforced in future by extending the comparative analysis between LST and screen-level temperature to other types of satellite products, as LANDSAT LST, and for other cities in the region.

Declaration of Competing Interest

The authors declare no conflict of interest.

Data availability

Data will be made available on request.

Acknowledgement

This work was supported by a grant of the Ministry of Research, Innovation and Digitization, CNCS - UEFISCDI, project number PN-III-P1-1.1-TE-2021-0882, within PNCDI III.

Supplementary materials

Supplementary material associated with this article can be found, in the online version, at [doi:10.1016/j.scs.2023.104568](https://doi.org/10.1016/j.scs.2023.104568).

References

- Alcoforado, M. J., & Andrade, H. (2006). Nocturnal urban heat island in Lisbon (Portugal): Main features and modelling attempts. *Theoretical and Applied Climatology*, 84(1), 151–159. <https://doi.org/10.1007/s00704-005-0152-1>
- Amani-Beni, M., Chen, Y., Vasileva, M., Zhang, B., & Xie, G. D. (2022). Quantitative-spatial relationships between air and surface temperature, a proxy for microclimate studies in fine-scale intra-urban areas? *Sustainable Cities and Society*, 77, Article 103584. <https://doi.org/10.1016/j.scs.2021.103584>
- Aniballe, R., Bonafoni, S., & Pichieri, M. (2014). Spatial and temporal trends of the surface and air heat island over Milan using MODIS data. *Remote Sensing of Environment*, 150, 163–171. <https://doi.org/10.1016/j.rse.2014.05.005>
- AppEEARS Team. (2021). Application for Extracting and Exploring Analysis Ready Samples (AppEEARS). Ver. 2.56. NASA EOSDIS Land Processes Distributed Active Archive Center (LP DAAC). Sioux Falls, South Dakota: USGS/Earth Resources Observation and

- Science (EROS) Center Accessed March 22, 2021 <https://lpdaacsvc.cr.usgs.gov/appears>.
- Azevedo, J. A., Chapman, L., & Muller, C. L. (2016). Quantifying the daytime and night-time urban heat island in Birmingham, UK: A comparison of satellite derived land surface temperature and high resolution air temperature observations. *Remote Sensing*, 8, 153. <https://doi.org/10.3390/rs8020153>
- Beck, C., Jacobite, J., & Jones, P. (2007). Frequency and within-type variations of large scale circulation types and their effects on low-frequency climate variability in central Europe since 1780. *International Journal of Climatology*, 27, 473–491. <https://doi.org/10.1002/joc.1410>
- Bisquert, M., Bordogna, G., Begue, A., et al. (2015). A simple fusion method for image time series based on the estimation of image temporal validity. *Remote Sensing*, 7(1), 704–724.
- Bisquert, M., Sanchez, J. M., & Caselles, V. (2016). Evaluation of disaggregation methods for downscaling MODIS land surface temperature to Landsat spatial resolution in Barrax test site. *IEEE Journal of Selected Topics in Applied Earth Observations and Remote Sensing*, 9(4), 1430–1438.
- Bisquert, M., Sanchez, J. M., Lopez-Urrea, R., et al. (2016). Estimating high resolution evapotranspiration from disaggregated thermal images. *Remote Sensing of Environment*, 187, 423–433.
- Chen, C., Li, D., & Keenan, T. (2021). Enhanced surface urban heat islands due to divergent urban-rural greening trends. *Environmental Research Letters*, 16, Article 124071. <https://doi.org/10.1088/1748-9326/ac36f8>
- Cheval, S., & Dumitrescu, A. (2009a). The July urban heat island of Bucharest as derived from Modis images. *Theoretical and Applied Climatology*, 96, 145–153. <https://doi.org/10.1007/s00704-008-0019-3>
- Cheval, S., Dumitrescu, A., & Bell, A. (2009b). The urban heat island of Bucharest during the extreme high temperatures of July 2007. *Theoretical and Applied Climatology*, 97 (3–4), 391–401. <https://doi.org/10.1007/s00704-008-0088-3>
- Cheval, S., & Dumitrescu, A. (2015). The summer surface urban heat island of Bucharest (Romania) retrieved from MODIS images. *Theoretical and Applied Climatology*, 121, 631–640. <https://doi.org/10.1007/s00704-014-1250-8>
- Cheval, S., Dumitrescu, A., Iraşoc, A., Paraschiv, M. G., Perry, M., & Ghent, D. (2022). MODIS-based climatology of the surface urban heat island at country scale (Romania). *Urban Climate*, 41, Article 101056. <https://doi.org/10.1016/j.ulclim.2021.101056>
- Clinton, N., & Gong, P. (2013). MODIS detected surface urban heat islands and sinks: Global locations and controls. *Remote Sensing of Environment*, 134, 294–304. <https://doi.org/10.1016/j.rse.2013.03.008>
- Copernicus Land Monitoring Service. (2018a). Urban Atlas. Available online: <http://land.copernicus.eu/local/urban-atlas/view> (accessed on 10 December 2022).
- Copernicus Land Monitoring Service. (2018b). Impervious Density. Available online: <https://land.copernicus.eu/pan-european/high-resolution-layers/imperviousness> (accessed on 10 December 2021).
- Crețu, Ş. C., Ichim, P., & Sfîcă, L. (2020). Summer urban heat island of Galați city (Romania) detected using satellite products. *Present Environment and Sustainable Development*, 14, 5–27. <https://doi.org/10.15551/pesd2020142001>
- Crețu, C., Ichim, P., Sfîcă, L., & Breabă, I. G. (2022). Relationship between land surface temperature and imperviousness density in the urban area of Iasi. In *Air and Water – Components of the Environment” Conference Proceedings* (pp. 12–18). Romania: Cluj-Napoca. https://doi.org/10.24193/AWC2022_02
- de Ridder, K., Maiheu, B., Lauwaet, D., Daglis, I., Keramitsoglou, I., Kourtidis, K., Manunta, P., & Paganini, M. (2017). Urban Heat Island intensification during hot spells – the case of Paris during the summer of 2003. *Urban Science*, 1, 3. <https://doi.org/10.3390/urbansci010003>
- Deilami, K., Kamruzzaman, M., & Liu, Y. (2018). Urban heat island effect: A systematic review of spatio-temporal factors, data, methods, and mitigation measures. *International Journal of Applied Earth Observation and Geoinformation*, 67, 30–42. <https://doi.org/10.1016/j.jag.2017.12.009>
- Fabrizi, R., Bonafoni, S., & Biondi, R. (2010). Satellite and ground-based sensors for the urban heat island analysis in the city of Rome. *Remote Sensing*, 2, 1400–1415. <https://doi.org/10.3390/rs2051400>
- Gago, E. J., Roldan, J., Pacheco-Torres, R., & Ordóñez, J. (2013). The city and urban heat islands: A review of strategies to mitigate adverse effects. *Renewable and Sustainable Energy Review*, 25, 749–758. <https://doi.org/10.1016/j.rser.2013.05.057>
- Gallo, K., & Krishnan, P. (2022). Evaluation of the bias in the use of clear-sky compared with all-sky observations of monthly and annual daytime Land Surface Temperature. *Journal of Applied Meteorology and Climatology*, 61. <https://doi.org/10.1175/JAMC-D-21-0240.1>
- Gao, F., Masek, J., Schwaller, M., et al. (2006). On the blending of the Landsat and MODIS surface reflectance: Predicting daily Landsat surface reflectance. *IEEE Transactions on Geoscience and Remote Sensing*, 44(8), 2207–2218.
- Georgiou, A., & Varnava, S. T. (2019). Evaluation of MODIS-derived LST products with air temperature measurements in Cyprus. *Geoplanning: Journal of Geomatics and Planning*, 6(1), 1–12. <https://doi.org/10.14710/geoplanning.6.1.1-12>
- Good, E. J. (2016). An in-situ-based analysis of the relationship between land surface “skin” and screen-level air temperatures. *Journal of Geophysical Research, [Atmospheres]*, 121, 8801–8819. <https://doi.org/10.1002/2016JD025318>
- Good, E. J., Aldred, F. M., Ghent, D. J., Veal, K. L., & Jimenez, C. (2022). An analysis of the stability and trends in the LST_CCI land surface temperature datasets over Europe. *Earth and Space Science*, 9, Article e2022EA002317. <https://doi.org/10.1029/2022EA002317>
- Guguman, I., & Cotrău, M. (1975). *Elements of urban climatology with examples from Romania (book in Romanian)*. Bucureşti: Romanian Academy Publishing House.
- Huang, W., Li, J., Guo, Q., Mansaray, L. R., Li, X., & Huang, J. (2017). A satellite-derived climatological analysis of urban heat island over Shanghai during 2000–2013. *Remote Sensing*, 9, 641. <https://doi.org/10.3390/rs9070641>
- Ichim, P., Apostol, L., Sfîcă, L., Kadhim-Abid, A. L., & Istrate, V. (2014). Frequency of thermal inversions between Siret and Prut rivers in 2013. *Present Environment and Sustainable Development*, 8(2), 267–285. <https://doi.org/10.2478/pesd-2014-0040>
- Ichim, P., & Sfîcă, L. (2020). The influence of urban climate on bioclimatic conditions in the city of Iași, Romania. *Sustainability*, 12, 9652. <https://doi.org/10.3390/su12229652>
- Imhoff, M. L., Zhang, P., Wolfe, R. E., & Bounoua, L. (2010). Remote sensing of the urban heat island effect across biomes in the continental USA. *Remote Sensing of Environment*, 114, 504–513. <https://doi.org/10.1016/j.rse.2009.10.008>
- Lamb, W. F., Creutzig, F., Callaghan, M. W., & Minx, J. (2019). Learning about urban climate solutions from case studies. *Natural Climate Change*, 9, 279–287. <https://doi.org/10.1038/s41558-019-0440-x>
- Li, L., Huang, X., Li, J., & Wen, D. (2017). Quantifying the spatiotemporal trends of canopy layer head island (CLHI) and its driving factors over Wuhan, China with satellite remote sensing. *Remote Sensing*, 9, 536. <https://doi.org/10.3390/rs9060536>
- Li, X., Zhou, Y., Asrar, G. R., Imhoff, M., & Li, X. (2017b). The surface urban heat island response to urban expansion: A panel analysis for the conterminous United States. *Science of the Total Environment*, 605, 426–435. <https://doi.org/10.1016/j.scitotenv.2017.06.229>
- Li, X., Zhou, Y., Asrar, G. R., & Zhu, Z. (2018). Developing a 1 km resolution daily air temperature dataset for urban and surrounding areas in the conterminous United States. *Remote Sensing of Environment*, 215, 74–84. <https://doi.org/10.1016/j.rse.2018.05.034>
- Li, H., Zhou, Y., Li, X., Meng, L., Wang, X., Wu, S., & Sodoudi, S. (2018b). A new method to quantify surface urban heat island intensity. *Science of the Total Environment*, 624, 262–272. <https://doi.org/10.1016/j.scitotenv.2017.11.360>
- Liu, Z., Zhan, W., Lai, J., Bechtel, B., Lee, X., Hong, F., Li, L., Huang, F., & Li, J. (2022). Taxonomy of seasonal and diurnal clear-sky climatology of surface urban heat island dynamics across global cities. *ISPRS Journal of Photogrammetry and Remote Sensing*. <https://doi.org/10.1010/j.isprsjprs.2022.02.19>
- Minea, I. (2010). The evaluation of the water chemistry and quality for the lakes from the south of the Hilly Plain of Jijia (Bahlui drainage basin). *Romanian Journal of Limnology: Lakes, Reservoirs Ponds*, 4(2), 131–144.
- Mirzaei, P. A., & Haghishat, F. (2010). Approaches to study urban heat island—Abilities and limitations. *Buildings and Environment*, 45, 2192–2201. <https://doi.org/10.1016/j.buildenv.2010.04.001>
- Mirzaei, P. A. (2015). Recent challenges in modeling of urban heat island. *Sustainable Cities and Society*, 19, 200–206. <https://doi.org/10.1016/j.scs.2015.04.001>
- Mohamed, A. A., Odindi, J., & Mutanga, O. (2017). Land surface temperature and emissivity estimation for urban heat island assessment using medium- and low-resolution space-borne sensors: A review. *Geocarto International*, 32, 455–470. <https://doi.org/10.1080/10106049.2016.1155657>
- Naserikia, M., Hart, M., Nazarian, N., & Bechtel, M. (2022). Background climates modulates the impact of land cover on urban surface temperature. *Scientific Reports*, 12, 15433. <https://doi.org/10.1038/s41598-022-19431-x>
- Nichol, J. E., Fung, W. Y., Lam, K. S., & Wong, M. S. (2009). Urban heat island diagnosis using ASTER satellite images and ‘in situ’ air temperature. *Atmospheric Research*, 94, 276–284. <https://doi.org/10.1016/j.atmosres.2009.06.011>
- Niță, I. A., Apostol, L., Patriche, C. V., Sfîcă, L., Bojarie, R., & Birsan, M. V. (2022). Frequency of atmospheric circulation types over romania according to jenkinson collision method based on two long-term reanalysis datasets. *Romanian Reports in Physics* Accessed at https://rjp.nipne.ro/accepted_papers.html.
- NOAA National Centers for Environmental Information (2001): Global Surface Hourly. NOAA National Centers for Environmental Information. Accessed on 1 of July 2022.
- Oke, T. R. (2006). *Initial guidance to obtain representative meteorological observations at urban sites* (p. 2004). Geneva, Switzerland: World Meteorological Organization. IOM Report No. 81, WMO/TD No. 1250Retrieved on 29 august 2007 from www.urban-climate.org/.
- O’Malley, C., Piroozfar, P., Farr, E. R. P., & Pompei, F. (2015). Urban Heat Island mitigating strategies: A case-based comparative analysis. *Sustainable Cities and Society*, 19, 222–235. <https://doi.org/10.1016/j.scs.2015.05.009>
- Patz, J. A., Campbell-Lendrum, D., Holloway, T., & Foley, J. A. (2005). Impact of regional climate change on human health. *Nature*, 438, 310–317. <https://doi.org/10.1038/nature04188>
- Peng, S., Piao, S., Ciais, P., Friedlingstein, P., Ottle, C., Breon, F.-M., Nan, H., Zhou, L., & Myneni, R. B. (2012). Surface urban heat island across 419 global big cities. *Environmental Science and Technology*, 46, 696–703. <https://doi.org/10.1021/es2030438>
- Peng, J., Ma, J., Liu, Q., Liu, Y., Hu, Y. N., Li, Y., & Yue, Y. (2018). Spatial-temporal change of land surface temperature across 285 cities in China: An urban-rural contrast perspective. *Science of Total Environment*, 635, 487–497. <https://doi.org/10.1016/j.scitotenv.2018.04.105>
- Philipp, A., Bartholy, J., & Beck, C. (2010). Cost733cat - a database of weather and circulation type classifications. *Physical Chemistry of Earth (Special Issue)*, 35, 360–373. <https://doi.org/10.1016/j.pce.2009.12.010>
- Philipp, A., Beck, C., Huth, R., et al. (2016). Development and comparison of circulation type classifications using the COST733 dataset and software. *International Journal of Climatology*, 36(7), 3673–3691. <https://doi.org/10.1002/joc.3920>
- Pichiari, M., Bonafoni, S., & Biondi, R. (2012). Satellite air temperature estimation for monitoring the canopy layer heat island of Milan. *Remote Sensing of Environment*, 127, 130–138. <https://doi.org/10.1016/j.rse.2012.08.025>
- Rao, P. (1972). *Remote sensing of urban heat islands from an environmental satellite*, 53 p. 647. Boston, MA: AMER Meteorological Soc, 45 Beacon St.

- Reis, C., Lopes, A., & Santos, N. (2022). Assessing urban heat island effects through local weather types in Lisbon's Metropolitan Area using big data from the Copernicus service. *Urban Climate*, 43, Article 101168. <https://doi.org/10.1016/j.ulclim.2022.101168>
- Rizwan, A. M., Dennis, L. Y. C., & Liu, C. (2008). A review on the generation, determination and mitigation of urban heat island. *Journal of Environmental Science*, 20, 120–128. [https://doi.org/10.1016/S1001-0742\(08\)60019-4](https://doi.org/10.1016/S1001-0742(08)60019-4)
- Roșu, L., & Blăgeanu, A. (2015). Evaluating performances of a public transport network in a post-socialist city using quantitative spatial approach. *Urbani Izziv*, 26(2), 103–116. <https://doi.org/10.5379/urbani-izziv-en-2015-26-02-002>
- Sandu, I., Pescaru, V. I., Poiana, I., & co-authors. (2008). *Climate of Romania*. Bucharest: Romanian Academy Publishing House.
- Santamouris, M., Cartalis, C., Synnefa, A., & Kolokotsa, D. (2015). On the impact of urban heat island and global warming on the power demand and electricity consumption of buildings—A review. *Energy and Buildings*, 98, 119–124. <https://doi.org/10.1016/j.enbuild.2014.09.052>
- Sfîcă, L., Iordache, L., Ichim, P., Leahu, A., Cazacu, M. M., Gurlui, S., & Trif, C. T. (2018b). The influence of weather conditions and local climate on particulate matter (PM10) concentration in metropolitan area of Iași, Romania. *Present Environment and Sustainable Development*, 11(2), 109–117. <https://doi.org/10.2478/pesd-2018-0029>
- Shachgedanova, M., Burt, T. P., & Davies, T. D. (1997). Some aspects of the three-dimensional heat islands in Moscow. *International Journal of Climatology*, 17(13), 1451–1465.
- Schwarz, N., Lautenbach, S., & Seppelt, R. (2011). Exploring indicators for quantifying surface urban heat islands of European cities with MODIS land surface temperatures. *Remote Sensing Environment*, 115(12), 3175–3186. <https://doi.org/10.1016/j.rse.2011.07.003>
- Seto, K. C., Güneralp, B., & Hutyra, L. R. (2012). Global forecasts of urban expansion to 2030 and direct impacts on biodiversity and carbon pools. *Proceedings of National Academy of Science of USA*, 109, 16083–16088. <https://doi.org/10.1073/pnas.121165810>
- Sfîcă, L., Ichim, P., Apostol, L., & Ursu, A. (2018a). The extent and intensity of the Urban Heat Island in Iași city, Romania. *Theoretical and Applied Climatology*, 134, 777–791. <https://doi.org/10.1007/s00704-017-2305-4>
- Shen, S., & Leptoukh, G. (2011). Estimation of surface air temperature over central and eastern Eurasia from MODIS land surface temperature. *Environmental Research Letters*, 6, Article 045206. <https://doi.org/10.1088/1748-9326/6/4/045206>
- Shepherd, J. M. (2005). A review of current investigations of urban-induced rainfall and recommendations for the future. *Earth Interactions*, 9, 1–27. <https://doi.org/10.1175/EI156.1>
- Silverman, B. W. (1986). *Density Estimation for Statistics and Data Analysis*. New York: Chapman and Hall.
- Sismanidis, P., Bechtel, B., Perry, M., & Ghent, D. (2022). The Seasonality of Surface Urban Heat Islands across Climates. *Remote Sensing*, 14, 2318. <https://doi.org/10.3390/rs14102318>
- Smoliak, B. V., Snyder, P. K., Twine, T. E., Mykley, P. M., & Hertel, W. F. (2015). Dense network observations of the twin cities canopy-layer urban heat island. *Journal of Applied Meteorology and Climatology*, 54, 1899–1917. <https://doi.org/10.1175/JAMC-D-14-0239.1>
- Sun, H., Chen, Y., & Zhan, W. (2015). Comparing surface- and canopy-layer urban heat islands over Beijing using MODIS data. *International Journal of Remote Sensing*, 36, 5448–5465. <https://doi.org/10.1080/01431161.2015.1101504>
- United Nations Department of Economic and Social Affairs. (2019). *World Urbanization Prospects: The 2018 Revision*. New York: United Nations.
- Utasi, Z., Pajtók-Tari, I., Mika, J., Patkós, C., & Tóth, A. (2012). Observed air pollution specifics of the valley-based towns. *Air and Water: Components of the environment*, 244–251.
- Venter, Z., Chakraborty, T., & Lee, X. (2021). Crowdsourced air temperatures contrast satellite measures of urban heat island and its mechanisms. *Science Advances*, 7, Eabb9569.
- Voogt, J. A., & Oke, T. R. (2003). Thermal remote sensing of urban climates. *Remote Sensing of Environment*, 86, 370–384. [https://doi.org/10.1016/S0034-4257\(03\)00079-8](https://doi.org/10.1016/S0034-4257(03)00079-8)
- Wan, Z., Zhang, Y., Wang, R., & Li, Z. L. (2001). *Early Land-Surface Temperature Product Retrieved from MODIS Data, 2001*. IGARSS.
- Wang, J., Huang, B., Fu, D., & Atkinson, P. M. (2015). Spatiotemporal variation in surface urban heat island intensity and associated determinants across major Chinese Cities. *Remote Sensing*, 7, 3670–3689. <https://doi.org/10.3390/rs70403670>
- Wang, K., Jiang, S., Wang, J., Zhou, C., Wang, X., & Lee, X. (2017). Comparing the diurnal and seasonal variabilities of atmospheric and surface urban heat islands based on the Beijing urban meteorological network. *Journal of Geophysical and Research Atmospheres*, 122, 2131–2154. <https://doi.org/10.1002/2016JD025304>
- Wang, Q., Wang, X., Zhou, Y., Liu, D., & Wang, H. (2022). The dominant factors and influence of urban characteristics on land surface temperature using random forest algorithm. *Sustainable Cities and Society*, 79, Article 103722. <https://doi.org/10.1016/j.scs.2022.103722>
- Wan, Z. (2019). *Collection-6 MODIS Land Surface Temperature Products Users' Guide*. ERI. University of California.
- Zhang, F., Cai, X., & Thornes, J. E. (2014). Birmingham's air and surface urban heat islands associated with Lamb weather types and cloudless anticyclonic conditions. *Progress in Physical Geography: Earth and Environment*, 38, 431–447. <https://doi.org/10.1177/030913314538725>
- Zhang, P., Bounoua, L., Imhoff, M. L., Wolfe, R. E., & Thome, K. (2014). Comparison of MODIS land surface temperature and air temperature over the continental USA meteorological stations. *Canadian Journal of Remote Sensing*, 40, 110–122. <https://doi.org/10.1080/07038992.2014.935934>
- Zhao, S., Zhou, D., & Liu, S. (2016). Data concurrency is required for estimating urban heat island intensity. *Environmental Pollution*, 208, 118–124. <https://doi.org/10.1016/j.envpol.2015.07.037>
- Zhou, B., Rybski, D., & Kropp, J. P. (2013). On the statistics of urban heat island intensity. *Geophysical Research Letters*, 40, 5486–5491. <https://doi.org/10.1002/2013GL057320>
- Zhou, D., Zhao, S., Zhang, L., & Liu, S. (2016). Remotely sensed assessment of urbanization effects on vegetation phenology in China's 32 major cities. *Remote Sensing of Environment*, 176, 272–281. <https://doi.org/10.1016/j.rse.2016.02.010>
- Zhou, B., Rybski, D., & Kropp, J. P. (2017). The role of city size and urban form in the surface urban heat island. *Scientific Report*, 7, 4791. <https://doi.org/10.1038/s41598-017-04242-2>
- Zhou, D., Bonafoni, S., Zhang, L., & Wang, R. (2018). Remote sensing of the urban heat island effect in a highly populated urban agglomeration area in East China. *Science and Total Environment*, 628–629, 415–429. <https://doi.org/10.1016/j.scitotenv.2018.02.074>